



# Boosting CO<sub>2</sub> hydrogenation to methanol by adding trace amount of Au into Cu/ZnO catalysts

Guiming Xie<sup>a</sup>, Rongrong Jin<sup>a,c</sup>, Pengju Ren<sup>b,c,\*</sup>, Yunming Fang<sup>a,\*\*</sup>, Runduo Zhang<sup>a</sup>, Zhou-jun Wang<sup>a,\*\*</sup>

<sup>a</sup> State Key Laboratory of Chemical Resource Engineering, Beijing Key Laboratory of Energy Environmental Catalysis, Beijing University of Chemical Technology, Beijing 100029, China

<sup>b</sup> State Key Laboratory of Coal Conversion, Institute of Coal Chemistry, Chinese Academy of Sciences, Taiyuan 030001, China

<sup>c</sup> National Energy Center for Coal to Liquids, Synfuels China Co., Ltd., Beijing 101400, China

## ARTICLE INFO

### Keywords:

Carbon dioxide  
CH<sub>3</sub>OH  
Copper  
Gold  
Bimetallic catalyst

## ABSTRACT

Boosted CO<sub>2</sub> hydrogenation to methanol was achieved by introducing appropriate amount of Au into conventional Cu-based catalysts. The Au<sub>x</sub>Cu/ZnO bimetallic catalysts with various Au/Cu molar ratio ( $x = 0.001, 0.005, 0.02$  and  $0.05$ ) were prepared by the co-precipitation method, among which the Au<sub>0.005</sub>Cu/ZnO catalyst exhibited the highest methanol production rate. The formation of Au-Cu alloy was identified on the Au<sub>x</sub>Cu/ZnO bimetallic catalysts. Experimental characterizations and density functional theory (DFT) calculations suggested metal-oxide interfaces with oxygen vacancies as intrinsic active sites for both un-promoted and Au-promoted Cu/ZnO catalysts. The promotion effect of Au in bimetallic catalysts was correlated with the increase of active sites, facilitation of CO<sub>2</sub> activation and modification of intermediate adsorption. The present work for the first time develops a promising Au<sub>0.005</sub>Cu/ZnO bimetallic catalyst with trace amount of Au (only 0.4 wt%) and provides insight into the reaction mechanism over Au-promoted Cu/ZnO catalysts for methanol synthesis via CO<sub>2</sub> hydrogenation.

## 1. Introduction

To tackle the threat of climate change resulting from the greenhouse effect, most of the countries have announced ambitious goals to achieve carbon neutrality within this century [1]. Among various greenhouse gases including carbon dioxide (CO<sub>2</sub>), methane (CH<sub>4</sub>), nitrous oxide (N<sub>2</sub>O) and fluorinated gases, CO<sub>2</sub> is the primary component in terms of both abundance and longevity [2]. As one of the carbon-negative technologies, catalytic conversion of CO<sub>2</sub> would play a critical role in targeting carbon neutrality [3–5]. On the other hand, methanol is an important chemical with wide applications as clean fuel or versatile building block [6]. Methanol synthesis via CO<sub>2</sub> hydrogenation using green hydrogen has gained increasing attention in recent years because this technology can not only convert greenhouse gas but also produce value-added chemical [7–9].

The industrialization of CO<sub>2</sub> hydrogenation to methanol is mainly impeded by the development of feasible catalysts. By virtue of high methanol synthesis rate, mild reaction conditions and acceptable

fabrication cost, copper (Cu)-based catalysts are most extensively studied and regarded to be most promising for industrial applications [10, 11]. However, both CO<sub>2</sub> conversion and methanol selectivity over current Cu-based catalysts are still unsatisfactory and novel structural modifications should be explored to improve their catalytic performance in CO<sub>2</sub> hydrogenation to methanol [12,13].

Recent studies have demonstrated that adding a second metal would significantly boost the methanol synthesis rate of Cu-based catalysts in CO<sub>2</sub> hydrogenation [14–18]. For example, Song's group observed higher CO<sub>2</sub> conversion and better methanol selectivity after introducing Pd into Cu/SiO<sub>2</sub> catalysts. The promotion effect in bimetallic catalysts was correlated with the formation of Pd-Cu alloy, which would enhance the adsorption of reactant molecules and promote the generation of formate intermediate [15,16]. Tada and co-workers improved methanol selectivity by adding Ag into a Cu-ZrO<sub>2</sub> catalyst, which was rationalized by the formation of Ag-Cu alloy as new active sites [17]. Tan *et al.* reported that the synergistic effect between Ni and Cu as well as the formation of oxygen vacancies endowed Ni-promoted Cu/CeO<sub>2</sub> catalysts with higher

\* Corresponding author at: State Key Laboratory of Coal Conversion, Institute of Coal Chemistry, Chinese Academy of Sciences, Taiyuan 030001, China.

\*\* Corresponding authors.

E-mail addresses: [renpengju@synfuelschina.com.cn](mailto:renpengju@synfuelschina.com.cn) (P. Ren), [fangym@mail.buct.edu.cn](mailto:fangym@mail.buct.edu.cn) (Y. Fang), [wangzj@mail.buct.edu.cn](mailto:wangzj@mail.buct.edu.cn) (Z.-j. Wang).

CO<sub>2</sub> conversion than the monometallic counterpart [18]. The above work document that constructing bimetallic Cu catalysts is an efficient strategy to boost the catalytic performance of Cu-based catalysts in CO<sub>2</sub> hydrogenation to methanol. Surprisingly, very limited studies have been reported on the use of AuCu bimetallic catalysts in this reaction although Au-based catalysts exhibited excellent methanol selectivity but poor CO<sub>2</sub> conversion [19,20].

Herein, Au-promoted Cu/ZnO catalysts with various Au/Cu molar ratio were synthesized by the classical co-precipitation method for CO<sub>2</sub> hydrogenation to methanol. The effect of Au introduction on catalytic performance of Cu/ZnO catalysts was investigated and the underlying structure-activity relationships were unraveled. The possible reaction mechanisms were proposed on the basis of in situ diffuse reflectance infrared Fourier transform spectroscopy (DRIFTS) experiments and density functional theory (DFT) calculations. To the best of our knowledge, this is the first report on the promotion effect of Au on Cu/ZnO catalysts for CO<sub>2</sub> hydrogenation to methanol.

## 2. Experimental section

### 2.1. Catalyst preparation and catalytic test

The metal precursors including Cu(NO<sub>3</sub>)<sub>2</sub>·3H<sub>2</sub>O (99.99 %), H<sub>2</sub>NaCl<sub>4</sub>·3H<sub>2</sub>O (99.9 %) and Zn(NO<sub>3</sub>)<sub>2</sub>·6H<sub>2</sub>O (99.99 %) as well as the precipitant agent of Na<sub>2</sub>CO<sub>3</sub> (99.99 %) were purchased from Aladdin and used as received. All the catalysts including monometallic (Cu/ZnO, Au/ZnO) and bimetallic (Au<sub>x</sub>Cu/ZnO) catalysts were prepared by the co-precipitation method. The detailed preparation protocol for the Cu/ZnO monometallic catalyst can be found in our previous work, wherein Cu/Zn molar ratio was set at 1/2 [7]. With a similar procedure, the Au<sub>x</sub>Cu/ZnO bimetallic catalysts (x = 0.001, 0.005, 0.02 and 0.05, denoting Au/Cu molar ratio) were prepared, wherein Cu/Zn molar ratio was set at 1/2 as well. Likewise, the Au/ZnO monometallic catalyst was prepared with the same nominal Au amount as that in the Au<sub>0.005</sub>Cu/ZnO catalyst.

The methanol synthesis reaction was carried out in a fixed bed reactor under 3.0 MPa at a weight hourly space velocity (WHSV) of 24,000 mL h<sup>-1</sup> g<sub>cat</sub><sup>-1</sup>. Specifically, 0.1 g catalyst granule was mixed with 0.4 g quartz sand and then packed into the stainless steel tube lined with a quartz tube (i.d. 6 mm). Prior to the reaction, the catalyst was reduced at 300 °C for 2 h in flowing H<sub>2</sub> (30 mL min<sup>-1</sup>). After the sample was cooled down to the reaction temperature, the reactant gases consisting of 10 mL min<sup>-1</sup> CO<sub>2</sub> and 30 mL min<sup>-1</sup> H<sub>2</sub> were introduced. The activity test was conducted in the temperature range of 200–275 °C with the data being acquired after 1.0 h time-on-stream at each temperature. The stability test was performed at 250 °C for 30 h. The products were analyzed using an online gas chromatograph (Fuli GC 9790Plus) equipped with both thermal conductivity detector (TCD) and flame ionized detector (FID). The CO<sub>2</sub> conversion, methanol selectivity and space time yield of methanol (STY<sub>MeOH</sub>) were calculated according to the following equations:

$$X_{\text{CO}_2} = \frac{F_{\text{CO}_2, \text{in}} - F_{\text{CO}_2, \text{out}}}{F_{\text{CO}_2, \text{in}}} \times 100 \%$$

$$S_{\text{MeOH}} = \frac{F_{\text{MeOH, out}}}{F_{\text{CO}_2, \text{in}} - F_{\text{CO}_2, \text{out}}} \times 100 \%$$

$$\text{STY}_{\text{MeOH}} = \frac{F_{\text{CO}_2, \text{in}} \times X_{\text{CO}_2} \times S_{\text{MeOH}} \times M_{\text{MeOH}}}{W_{\text{cat}}}$$

where *F*, *M* and *W* represent the molar flow rate, molar mass and weight, respectively.

### 2.2. Structural characterizations and computational methods

The details were elaborated in [Supplementary material](#).

## 3. Results and discussion

### 3.1. Catalytic activity

Fig. 1 shows CO<sub>2</sub> conversion, methanol selectivity and STY<sub>MeOH</sub> over monometallic (Cu/ZnO, Au/ZnO) and bimetallic (Au<sub>x</sub>Cu/ZnO, x = 0.001, 0.005, 0.02 and 0.05) catalysts in typical reaction temperature range for CO<sub>2</sub> hydrogenation to methanol. Over all the investigated catalysts, CO was detected as the main byproduct at various reaction temperatures. Negligible amount of methane was detected at 275 °C with selectivity lower than 0.1 %. In general, the Cu/ZnO monometallic catalyst exhibited favorable CO<sub>2</sub> conversion and methanol selectivity, whereas the Au/ZnO monometallic catalyst had the lowest CO<sub>2</sub> conversion but the highest methanol selectivity. The Cu/ZnO monometallic catalyst possessed much higher STY<sub>MeOH</sub> than the Au/ZnO monometallic catalyst at various reaction temperature. Such observations were consistent with those reported in the literature for the Cu/ZnO and Au/ZnO monometallic catalysts [9–11,19,20]. In comparison with the Cu/ZnO monometallic catalyst, the Au<sub>x</sub>Cu/ZnO bimetallic catalysts delivered close CO<sub>2</sub> conversion but boosted methanol selectivity and STY<sub>MeOH</sub>. Moreover, the catalytic activity of the Au<sub>x</sub>Cu/ZnO bimetallic catalysts depended critically on Au/Cu molar ratio. Evident improvement in CO<sub>2</sub> conversion was noticed on the Au<sub>0.001</sub>Cu/ZnO and Au<sub>0.005</sub>Cu/ZnO catalysts, whereas little enhancement in CO<sub>2</sub> conversion was observed on the Au<sub>0.02</sub>Cu/ZnO and Au<sub>0.05</sub>Cu/ZnO catalysts (Fig. 1a). All the Au<sub>x</sub>Cu/ZnO bimetallic catalysts exhibited much higher methanol selectivity than the Cu/ZnO monometallic catalyst, wherein methanol selectivity first increased and then decreased with the rise of Au/Cu molar ratio (Fig. 1b). Except the Au<sub>0.05</sub>Cu/ZnO catalyst at 200 °C, all the other Au<sub>x</sub>Cu/ZnO bimetallic catalysts possessed much higher STY<sub>MeOH</sub> than the Cu/ZnO monometallic catalyst, wherein STY<sub>MeOH</sub> showed a similar trend as methanol selectivity with the increase of Au/Cu molar ratio (Fig. 1c).

The above results clearly demonstrate that introducing appropriate amount of Au would substantially improve methanol selectivity and STY<sub>MeOH</sub> of Cu/ZnO catalysts. The Au<sub>0.005</sub>Cu/ZnO catalyst showed the highest STY<sub>MeOH</sub> among all the investigated catalysts. Specifically, STY<sub>MeOH</sub> at 250 °C was 179.7, 314.4 and 32.8 g<sub>MeOH</sub> kg<sub>cat</sub><sup>-1</sup> h<sup>-1</sup> on the Cu/ZnO, Au<sub>0.005</sub>Cu/ZnO and Au/ZnO catalysts, respectively. That is, the methanol production rate on the Au<sub>0.005</sub>Cu/ZnO catalyst was 1.75 times as high as that on the Cu/ZnO catalyst. Furthermore, the Au<sub>0.005</sub>Cu/ZnO catalyst exhibited outstanding STY<sub>MeOH</sub> among various Cu-based catalysts under similar reaction conditions (Table S1) [15,17,18].

To further elucidate the promotional role of Au on Cu/ZnO catalysts, the apparent activation energy (*E<sub>a</sub>*) of CO<sub>2</sub> conversion was determined using Arrhenius law under differential reaction conditions. As Fig. S1 demonstrates, the *E<sub>a</sub>* on the Au<sub>0.005</sub>Cu/ZnO catalyst (37.1 kJ mol<sup>-1</sup>) was markedly lower than that on the Cu/ZnO catalyst (43.7 kJ mol<sup>-1</sup>). This kinetic characterization suggests that CO<sub>2</sub> conversion and thus methanol formation of Cu/ZnO catalysts were efficiently promoted by introducing appropriate amount of Au. It is worth mentioning that the content of Au in the Au<sub>0.005</sub>Cu/ZnO catalyst was only 0.4 wt%. Such a trace amount of Au would favor the industrialization of the AuCu bimetallic catalysts in the future.

### 3.2. Catalyst characterization

To acquire the structure-activity relationships of Au-promoted Cu/ZnO catalysts, structural characterizations were systematically carried out. Fig. S2 presents N<sub>2</sub> adsorption-desorption isotherms of the reduced catalysts, wherein the specific surface area (*S<sub>BET</sub>*) of each sample was designated. Generally, all the isotherms displayed similar type IV shape with H3 hysteresis loops, suggesting the presence of mesopores [21]. Comparatively, the introduction of Au increased *S<sub>BET</sub>* of Cu/ZnO catalysts. The Au<sub>0.005</sub>Cu/ZnO catalyst exhibited the highest *S<sub>BET</sub>* among the bimetallic catalysts, which is consistent with the trend in methanol

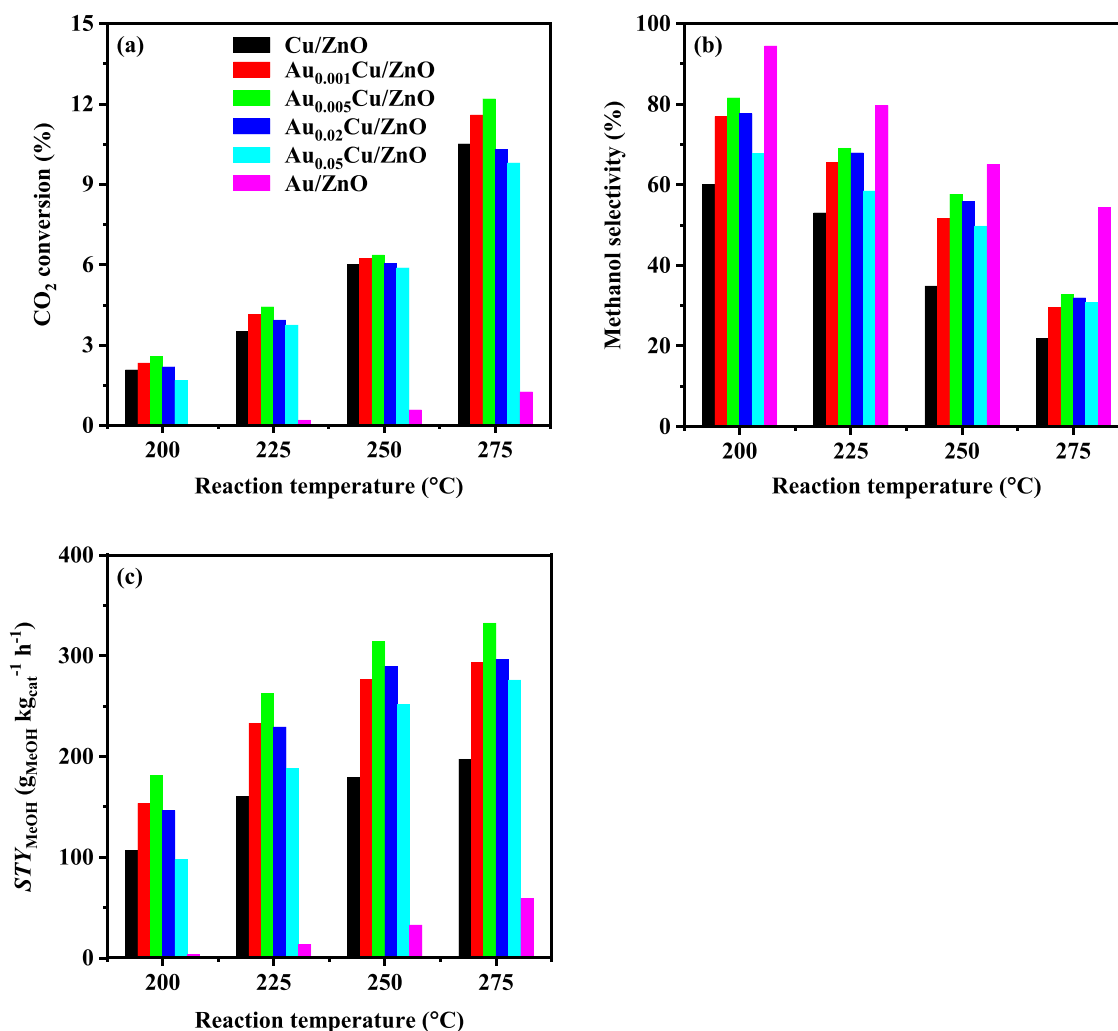


Fig. 1. CO<sub>2</sub> conversion (a), methanol selectivity (b) and STY<sub>MeOH</sub> (c) over various catalysts at 200–275 °C under 3.0 MPa.

production rate. The increased  $S_{\text{BET}}$  on the bimetallic catalysts would promote the dispersion of active metals, conducive to methanol synthesis [9–13]. Besides, the Au/ZnO catalyst showed higher  $S_{\text{BET}}$  than Cu-containing catalysts, which could be readily rationalized by the much lower metal content on the former sample.

Fig. 2 shows XRD patterns of the reduced catalysts. Diffraction peaks corresponding to hexagonal wurtzite ZnO phases were found on all the catalysts. Reflections originating from metallic Cu were identified on the Cu/ZnO and Au<sub>x</sub>Cu/ZnO catalysts. In contrast, no recognizable features relating to Au-containing phases were noticed on the Au<sub>x</sub>Cu/ZnO and Au/ZnO catalysts, which should be due to the ultra-low Au loading [22]. According to Scherrer equation using Cu(111) reflections, Cu crystallite size on the Cu/ZnO, Au<sub>0.001</sub>Cu/ZnO, Au<sub>0.005</sub>Cu/ZnO, Au<sub>0.02</sub>Cu/ZnO and Au<sub>0.05</sub>Cu/ZnO catalysts was estimated as 24.8, 18.8, 18.4, 22.7 and 23.7 nm, respectively. That is, the introduction of Au would decrease the crystallite size of Cu nanoparticles on Cu/ZnO catalysts, which would yield higher active surface area and lead to better methanol synthesis activity [13,23].

The catalyst morphology and metal dispersion were characterized by TEM images. As displayed in Fig. 3, nanoscale patches corresponding to ZnO support were observed on all the catalysts. Notably, Cu and Au nanoparticles showed different contrast with ZnO patches as the reference. In detail, Cu nanoparticles were difficult to be discriminated from ZnO patches on the Cu/ZnO and Au<sub>x</sub>Cu/ZnO catalysts, which was widely reported in the literature as well [7,24,25]. On the contrary, Au nanoparticles could be readily discerned on the Au/ZnO catalyst owing

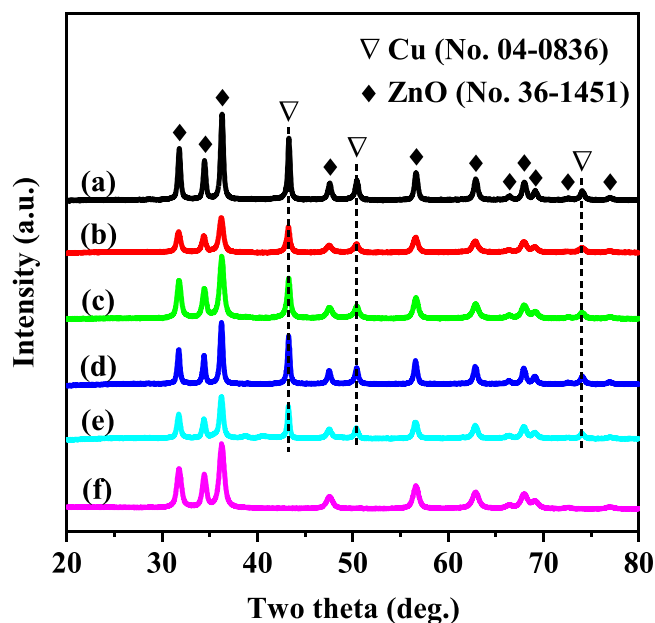
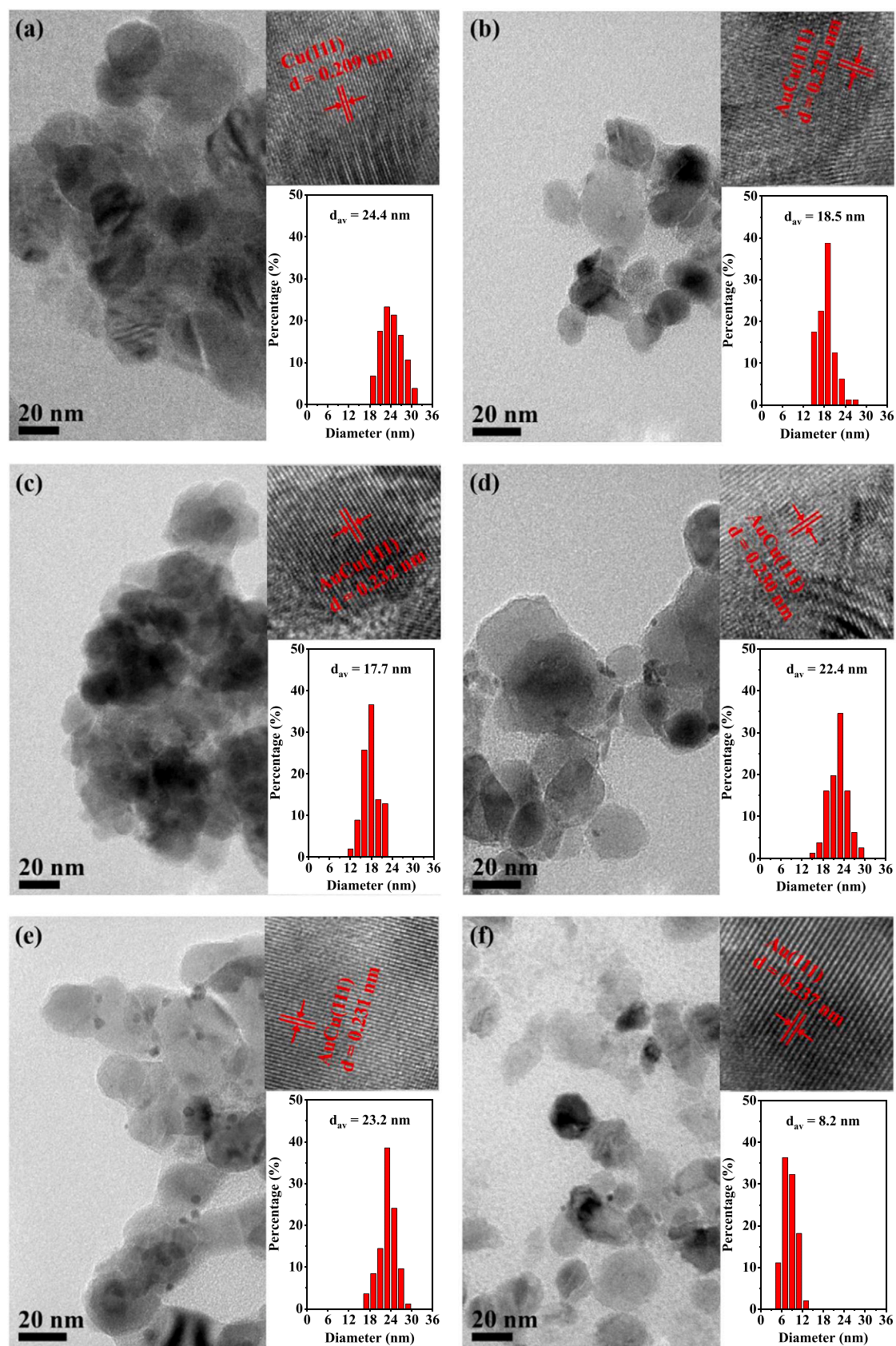


Fig. 2. XRD patterns of the reduced catalysts. (a) Cu/ZnO; (b) Au<sub>0.001</sub>Cu/ZnO; (c) Au<sub>0.005</sub>Cu/ZnO; (d) Au<sub>0.02</sub>Cu/ZnO; (e) Au<sub>0.05</sub>Cu/ZnO; and (f) Au/ZnO.



**Fig. 3.** TEM images and metal size distribution histograms of the reduced catalysts. (a) Cu/ZnO; (b)  $\text{Au}_{0.001}\text{Cu/ZnO}$ ; (c)  $\text{Au}_{0.005}\text{Cu/ZnO}$ ; (d)  $\text{Au}_{0.02}\text{Cu/ZnO}$ ; (e)  $\text{Au}_{0.05}\text{Cu/ZnO}$ ; and (f) Au/ZnO.

to the distinct contrast between Au and ZnO. By carefully examining TEM images of the  $\text{Au}_x\text{Cu}/\text{ZnO}$  catalysts, it is noticed that Au nanoparticles existing as tiny black dots emerged on the  $\text{Au}_{0.02}\text{Cu}/\text{ZnO}$  and  $\text{Au}_{0.05}\text{Cu}/\text{ZnO}$  catalysts. Such a phenomenon was not prominent on the  $\text{Au}_{0.001}\text{Cu}/\text{ZnO}$  and  $\text{Au}_{0.005}\text{Cu}/\text{ZnO}$  catalysts. This observation suggests that introducing excessive Au into Cu/ZnO catalysts would result in separate Au nanoparticles. With the lattice distance being calculated from HR-TEM images, Cu-containing nanoparticles were recognized and their size distributions were determined on the Cu/ZnO and  $\text{Au}_x\text{Cu}/\text{ZnO}$  catalysts. As Fig. 3(a-e) show, the lattice distance of Cu(111) planes was evidently enlarged after introduction of Au, which suggested an effective alloying between Au and Cu on the  $\text{Au}_x\text{Cu}/\text{ZnO}$  catalysts [26,27]. The average metal size on the Cu/ZnO,  $\text{Au}_{0.001}\text{Cu}/\text{ZnO}$ ,  $\text{Au}_{0.005}\text{Cu}/\text{ZnO}$ ,  $\text{Au}_{0.02}\text{Cu}/\text{ZnO}$  and  $\text{Au}_{0.05}\text{Cu}/\text{ZnO}$  catalysts was estimated as 24.4, 18.5, 17.7, 22.4 and 23.2 nm, respectively. In consistent with XRD results, TEM data reveal the enhancement of metal dispersion after introducing Au into Cu/ZnO catalysts. Besides, well dispersed Au nanoparticles with an average size of 8.2 nm were observed on the Au/ZnO catalyst (Fig. 3f).

To gain more insight into the microstructure of the  $\text{Au}_x\text{Cu}/\text{ZnO}$  bimetallic catalysts, the  $\text{Au}_{0.005}\text{Cu}/\text{ZnO}$  catalyst was further characterized with HR-TEM images and EDX elemental mapping. As HR-TEM images in Figs. S3a and S3b demonstrate, abundant metal-oxide interfaces were formed on the  $\text{Au}_{0.005}\text{Cu}/\text{ZnO}$  catalyst. It has been widely

reported that metal-oxide interfaces play a crucial role in methanol synthesis over Cu-based catalysts [7,28,29]. Generally, two effects have been proposed to rationalize the exceptional methanol synthesis activity on metal-oxide interfaces. One is called bifunctional effect, wherein both metal and oxide participate in the adsorption and activation of reactants. The other is called electronic effect, wherein special electronic properties are developed at the interface resulting from appropriate metal-oxide interactions. Both effects may change the adsorption mode of reactants, leading to more favorable transformation processes for methanol synthesis. As a matter of fact, it is difficult to disentangle these two effects which may function concurrently. The  $\text{Au}_{0.005}\text{Cu}/\text{ZnO}$  catalyst has higher metal dispersion than the Cu/ZnO and other  $\text{Au}_x\text{Cu}/\text{ZnO}$  catalysts, which would result in more abundant metal-oxide interfaces and thus better methanol synthesis activity. As EDX elemental mapping in Figs. S3(c-f) documents, Au and Cu were homogeneously alloyed on the  $\text{Au}_{0.005}\text{Cu}/\text{ZnO}$  catalyst. The formation of Au-Cu alloy may modulate the activation of reactant molecules or conversion of reaction intermediates, leading to enhanced methanol synthesis activity on the bimetallic catalysts.

The chemical state and surface composition of the reduced catalysts were examined by XPS and AES spectra. Shown in Fig. 4 are Cu 2p, Au 4f and O 1s XPS spectra of the reduced Cu/ZnO,  $\text{Au}_{0.005}\text{Cu}/\text{ZnO}$ ,  $\text{Au}_{0.02}\text{Cu}/\text{ZnO}$  and Au/ZnO catalysts. For Cu 2p XPS spectra (Fig. 4a), characteristic features corresponding to metallic Cu were observed on the Cu/ZnO

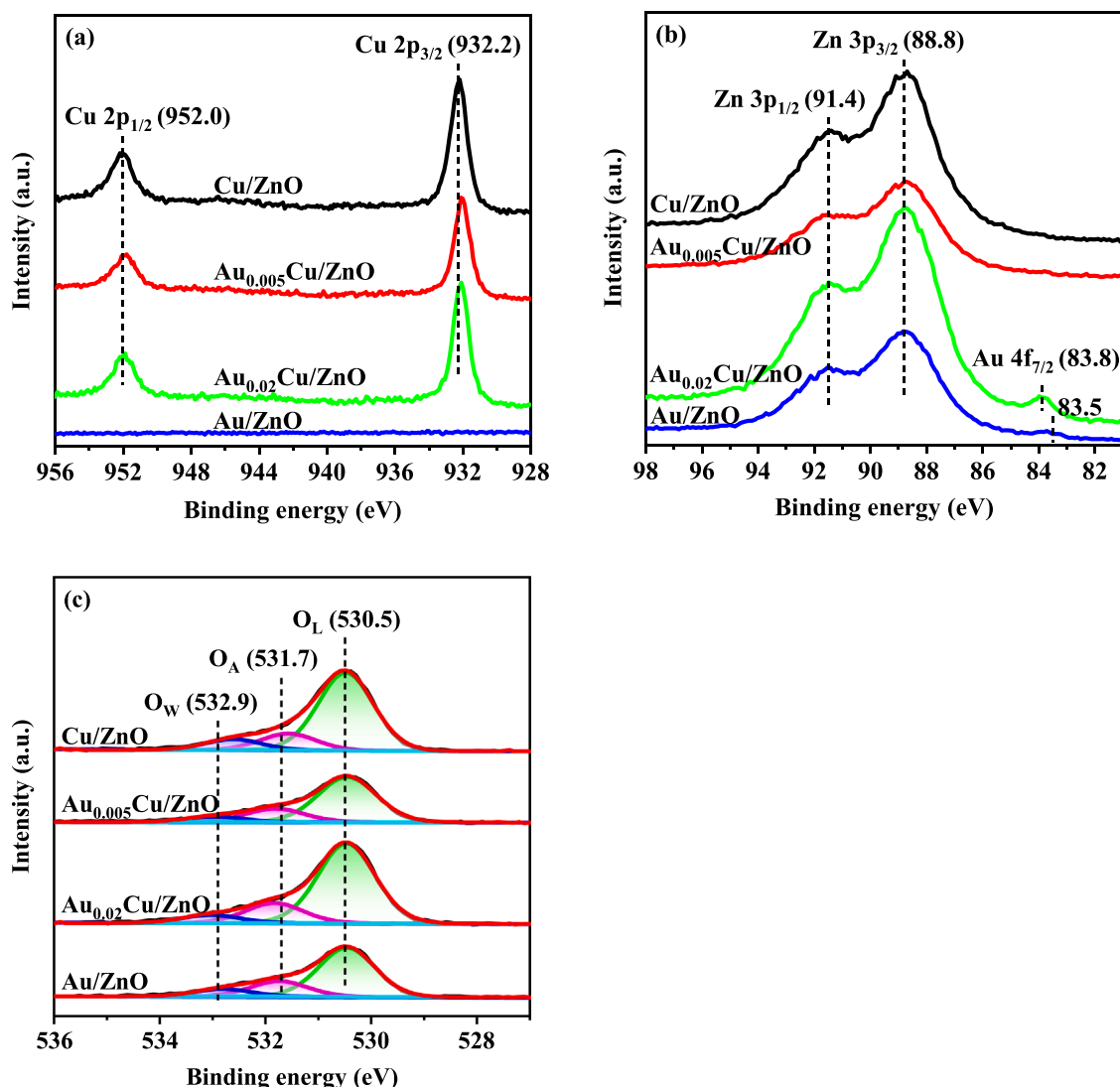


Fig. 4. XPS spectra of the reduced catalysts. (a) Cu 2p; (b) Au 4f; and (c) O 1s.

catalyst, wherein Cu 2p<sub>3/2</sub> and Cu 2p<sub>1/2</sub> peaks located at 932.2 and 952.0 eV respectively [7,30]. After introduction of Au, a negative shift in binding energy was noticed on both Au<sub>0.005</sub>Cu/ZnO and Au<sub>0.02</sub>Cu/ZnO catalysts. For Au 4f XPS spectra (Fig. 4b), data analysis was complicated by the fact that Au 4f<sub>5/2</sub> peaks (around 87.0 eV) were totally overlapped by Zn 3p<sub>3/2</sub> peaks (in the range of 85.0–90.0 eV). A distinct Au 4f<sub>7/2</sub> peak was detected on the Au<sub>0.02</sub>Cu/ZnO and Au/ZnO catalysts at 83.8 and 83.5 eV respectively. Compared with the Au/ZnO monometallic catalyst, a positive shift in binding energy was noticed on the Au<sub>0.02</sub>Cu/ZnO bimetallic catalyst. The opposite binding energy shifts between Cu 2p and Au 4f after introducing Au into Cu/ZnO catalysts provide further evidence for the formation of Au-Cu alloy on the Au<sub>x</sub>Cu/ZnO bimetallic catalysts. A broad peak was found on O 1s XPS spectra of all the catalysts, which could be deconvoluted into three features (Fig. 4c). According to the literature, three O 1s peaks around 530.5, 531.7 and 532.9 eV were ascribed as lattice oxygen (O<sub>L</sub>), adsorbed oxygen (O<sub>A</sub>) and water species (O<sub>W</sub>), respectively [31–33]. The O<sub>A</sub>/O<sub>L</sub> concentration ratio was generally employed to describe the concentration of oxygen vacancies. As compiled in Table S2, the Au<sub>x</sub>Cu/ZnO bimetallic catalysts possessed much higher O<sub>A</sub>/O<sub>L</sub> than the Cu/ZnO catalyst. That is, oxygen vacancies were effectively induced after introducing Au into Cu/ZnO catalysts. The enriched oxygen vacancies would facilitate CO<sub>2</sub> activation and thus boost methanol synthesis activity [6,10,11,18]. Given the difficulty in distinguishing Cu<sup>0</sup> from Cu<sup>+</sup> by Cu 2p XPS spectra, Cu LMM AES spectra were further collected. As confirmed in Fig. S4, most of Cu species existed as metallic state over the reduced Cu/ZnO and Au<sub>x</sub>Cu/ZnO catalysts. Notably, the enriched oxygen vacancies on the Au<sub>x</sub>Cu/ZnO catalysts exerted little influence on the chemical state of Cu species although the generation of oxygen vacancies would introduce extra electrons into the system. It is worth mentioning that oxygen vacancies are always generated on ZnO in a localized manner. The impact of extra electrons on the chemical state of Cu species would thus be indirect and limited. Moreover, the chemical state of Cu species may also be affected by other structural parameters, such as alloying formation, metal size and metal-support interactions, which makes the interpretation of XPS/Auger data complicated.

The metal-support interactions of the Cu/ZnO, Au<sub>x</sub>Cu/ZnO and Au/ZnO catalysts were characterized by H<sub>2</sub>-TPR profiles. As illustrated in Fig. 5a, a relatively broad reduction peak at 205 °C was observed on the Cu/ZnO catalyst, which resulted from the reduction of CuO species [34]. A sharp reduction peak in the range of 185–200 °C was detected on the Au<sub>x</sub>Cu/ZnO bimetallic catalysts, which originated from the reduction of Au-Cu alloy. Comparatively, the reduction temperature on the Au<sub>x</sub>Cu/ZnO bimetallic catalysts was lower than that on the Cu/ZnO

monometallic catalyst. Moreover, the reduction temperature on the Au<sub>x</sub>Cu/ZnO bimetallic catalysts first decreased and then increased as Au/Cu molar ratio rose. It has been generally acknowledged that on Cu-based catalysts, the lower reduction temperature reflects the stronger metal-support interactions [18,23]. Therefore, H<sub>2</sub>-TPR profiles document intensified metal-support interactions by introduction of Au into Cu/ZnO catalysts, which rationalized the smaller metal particle size on the Au<sub>x</sub>Cu/ZnO bimetallic catalysts [35]. Besides, a weak but unambiguous reduction peak at 154 °C was found on the Au/ZnO catalyst, which was ascribed to the reduction of oxidized gold species [36,37]. The much lower intensity of reduction peak on the Au/ZnO catalyst should relate with its ultra-low metal amount.

The surface basicity of the Cu/ZnO, Au<sub>x</sub>Cu/ZnO and Au/ZnO catalysts was analyzed by CO<sub>2</sub>-TPD characterizations. As depicted in Fig. 5b, several desorption peaks were observed on each catalyst. On the basis of desorption temperature, these desorption peaks can be classified into three regions corresponding to weak (<150 °C), medium (150–550 °C) and strong (>550 °C) basic sites, respectively [38–40]. Among them, the medium basic sites are generally regarded as the primary sites responsible for CO<sub>2</sub> activation in methanol synthesis [39,40]. Quantitatively, the concentration of the medium basic sites on the Cu/ZnO, Au<sub>0.001</sub>Cu/ZnO, Au<sub>0.005</sub>Cu/ZnO, Au<sub>0.02</sub>Cu/ZnO, Au<sub>0.05</sub>Cu/ZnO and Au/ZnO catalysts was 0.050, 0.107, 0.205, 0.082, 0.056 and 0.076 mmol g<sup>-1</sup>, respectively. It is noted that the medium basic sites of Cu/ZnO catalysts were substantially developed after introduction of Au, which would promote CO<sub>2</sub> activation and thus boost methanol synthesis activity. The enrichment of medium basic sites by the incorporation of Au could mainly be attributed to three aspects. First, the introduction of Au increases the specific surface area of Cu/ZnO catalysts, which would expose more basic sites [38]. Second, the introduction of Au modulates metal size and metal-oxide interfaces, which would tune the adsorption of CO<sub>2</sub> [16,39]. Third, the introduction of Au yields extra oxygen vacancies, which would provide more active sites for CO<sub>2</sub> adsorption [23, 41].

To summarize, structural characterizations reveal the formation of Au-Cu alloy and the modification of physicochemical properties after introducing Au into Cu/ZnO catalysts. In comparison with the Cu/ZnO monometallic catalyst, the Au<sub>x</sub>Cu/ZnO bimetallic catalysts exhibited higher S<sub>BET</sub>, smaller metal particle size, enriched oxygen vacancies, stronger metal-support interactions and increased medium basic sites. These structural modifications would generate more active sites, promote CO<sub>2</sub> activation and modify intermediate conversion, synergistically leading to boosted methanol synthesis activity [10,11,14–18,41]. Notably, excessive introduction of Au would yield unalloyed Au, which

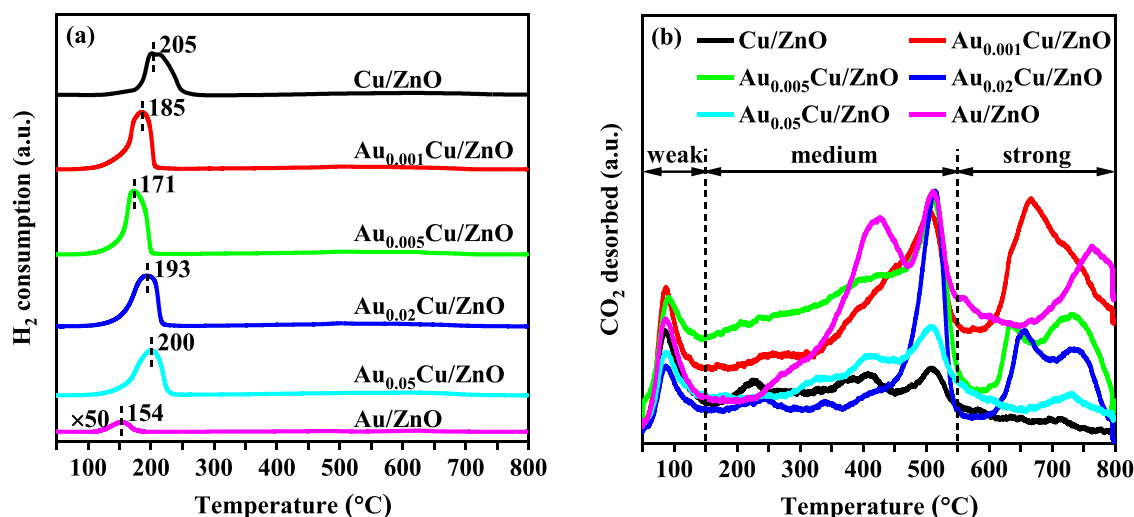


Fig. 5. (a) H<sub>2</sub>-TPR profiles of the calcined catalysts and (b) CO<sub>2</sub>-TPD profiles of the reduced catalysts.

may cover some of the Cu active sites, weaken the modification function and thus regress methanol synthesis activity on the  $\text{Au}_x\text{Cu}/\text{ZnO}$  bimetallic catalysts [14,42].

### 3.3. Mechanistic studies

To gain in-depth insight into the promotion effect of trace Au on Cu/ZnO catalysts, the mechanistic studies were carried out by combining in situ DRIFTS experiments and comprehensive DFT calculations. Fig. 6 compares in situ DRIFTS spectra between the Cu/ZnO and  $\text{Au}_{0.005}\text{Cu}/\text{ZnO}$  catalysts as a function of reaction time at 250 °C. On both catalysts, distinct features could be observed after 1 min of reaction, which slightly grew as the reaction proceeded. Specifically, three kinds of reaction intermediates were identified on the Cu/ZnO catalyst. The bands at 1580, 1412 and 1368  $\text{cm}^{-1}$  were attributed to  $^*\text{HCOO}$  (formate) species [9,43,44]. The bands at 1456, 1187 and 1134  $\text{cm}^{-1}$  were assigned to  $^*\text{b-OCH}_3$  (bridged methoxy) species [45–47]. The band at 1050  $\text{cm}^{-1}$  was ascribed to  $^*\text{t-OCH}_3$  (terminal methoxy) species [45–47]. In contrast, only two kinds of reaction intermediates including  $^*\text{HCOO}$  and  $^*\text{b-OCH}_3$  species were detected on the  $\text{Au}_{0.005}\text{Cu}/\text{ZnO}$  catalyst. In situ DRIFTS spectra demonstrate that both Cu/ZnO and  $\text{Au}_{0.005}\text{Cu}/\text{ZnO}$  catalysts adopted a formate pathway in methanol synthesis, which is consistent with previous studies over Cu/ZnO catalysts [7,24,29]. Notably, the adsorption configuration of methoxy species was altered by the addition of Au. Only  $^*\text{b-OCH}_3$  species was detected on the  $\text{Au}_{0.005}\text{Cu}/\text{ZnO}$  catalyst, whereas both  $^*\text{b-OCH}_3$  and  $^*\text{t-OCH}_3$  species were found on the Cu/ZnO catalyst. Cop  ret et al. substantiated the formate and methoxy species as the critical reaction intermediates in  $\text{CO}_2$  hydrogenation to methanol over Cu/ZrO<sub>2</sub> catalysts [29]. Moreover, Wang and co-workers documented the reaction route involving the formation of  $^*\text{b-OCH}_3$  species was more effective than that involving the formation of  $^*\text{t-OCH}_3$  species in methanol synthesis over copper-cerium-zirconium catalysts [46]. The exclusive configuration of  $^*\text{b-OCH}_3$  species on the  $\text{Au}_{0.005}\text{Cu}/\text{ZnO}$  catalyst would be closely related to the boosted methanol synthesis activity on the bimetallic catalyst.

To understand the reaction mechanism at a molecule level, DFT calculations were further conducted. First, the impact of Au addition on the formation of oxygen vacancies was simulated. As illustrated in Fig. S5, the initial state of the Cu/ZnO and  $\text{Au}_x\text{Cu}/\text{ZnO}$  catalysts was simulated by the ZnO/Cu(111) and ZnO/Au-Cu(111) models respectively, wherein an inverse model was employed to describe the unique structural motif at the metal/oxide interface of Cu-based catalysts. The choice of an inverse model was mainly based upon two considerations. First, serious complexity and uncertainty were encountered in the conventional model due to the complicated ZnO surface, which was

perfectly circumvented in the inverse model. Second, various research groups have documented that the inverse model would serve as a proper model structure for Cu-based catalysts in methanol synthesis [28, 48–50]. In addition, the state of the Cu/ZnO and  $\text{Au}_x\text{Cu}/\text{ZnO}$  catalysts after generating oxygen vacancies by  $\text{H}_2$  reduction was simulated by the  $\text{ZnO}_{1-x}/\text{Cu}(111)$  and  $\text{ZnO}_{1-x}/\text{Au-Cu}(111)$  models respectively (Fig. 7). The corresponding reaction energy ( $E_r$ ) of oxygen vacancy formation was calculated to estimate the tendency to generate oxygen vacancies on the catalyst surface. As compiled in Table S3, the  $E_r$  of oxygen vacancy formation on the ZnO/Au-Cu(111) surface (−0.96 eV) was considerably lower than that on the ZnO/Cu(111) surface (−0.30 eV). That is, the introduction of Au would considerably induce the formation of oxygen vacancies on Cu/ZnO catalysts, in support of XPS data.

Second, the promotion effect of Au addition on the reaction process was investigated. According to in situ DRIFTS results in the present work and relevant studies in the literature,  $\text{CO}_2$  hydrogenation to methanol over Cu/ZnO and  $\text{Au}_x\text{Cu}/\text{ZnO}$  catalysts should proceed with a formate pathway. Very recently, Liu and co-workers conducted a holistic study on the reaction pathway over ZnO/Cu inverse model catalysts. It was revealed that the  $^*\text{HCOO}$  intermediate was formed by attacking the adsorbed  $^*\text{CO}_2$  with the dissociated  $^*\text{H}$  atoms [50]. The formed  $^*\text{HCOO}$  intermediate was successively hydrogenated into  $^*\text{H}_2\text{COO}$ ,  $^*\text{H}_2\text{COOH}$ ,  $^*\text{H}_2\text{CO}$  and  $^*\text{CH}_3\text{O}$  intermediates before the production of methanol. On the basis of such a reaction pathway, the reaction energy profiles of  $\text{CO}_2$  hydrogenation to methanol over various models could be calculated. To mimic oxygen vacancy characteristic of the Cu/ZnO and  $\text{Au}_x\text{Cu}/\text{ZnO}$  catalysts, the ZnO/Cu(111) and  $\text{ZnO}_{1-x}/\text{Au-Cu}(111)$  models were established as the start surface for the Cu/ZnO and  $\text{Au}_x\text{Cu}/\text{ZnO}$  catalysts respectively. Fig. 8 compares the reaction energy profiles on the ZnO/Cu(111),  $\text{ZnO}_{1-x}/\text{Au-Cu}(111)$  and  $\text{ZnO}_{1-x}/\text{Cu}(111)$  surface, wherein the  $\text{ZnO}_{1-x}/\text{Cu}(111)$  surface served as a reference model. In comparison with the reference model of the  $\text{ZnO}_{1-x}/\text{Cu}(111)$  surface, the  $\text{ZnO}_{1-x}/\text{Au-Cu}(111)$  surface exhibited similar energy profiles, suggesting limited influence of Au dopant on the conversion of reactants and intermediates. In contrast, the  $\text{ZnO}_{1-x}/\text{Au-Cu}(111)$  and  $\text{ZnO}_{1-x}/\text{Cu}(111)$  surface with oxygen vacancies exhibited much lower relative energy ( $\Delta E$ ) than the ZnO/Cu(111) surface without oxygen vacancies, highlighting the promotional effect of oxygen vacancies on the conversion of reactants and intermediates. To check the possibility of dissociation of  $\text{CO}_2$  by oxygen vacancies, the reaction energy profiles of  $\text{CO}_2$  adsorption and activation on the  $\text{ZnO}_{1-x}/\text{Au-Cu}(111)$  surface have been further calculated. As shown in Fig. S6, formate formation route was much more favorable than  $\text{CO}_2$  dissociation route. That is, oxygen vacancies would not induce  $\text{CO}_2$  dissociation. The above calculations demonstrate that the introduction of Au into Cu/ZnO catalysts would

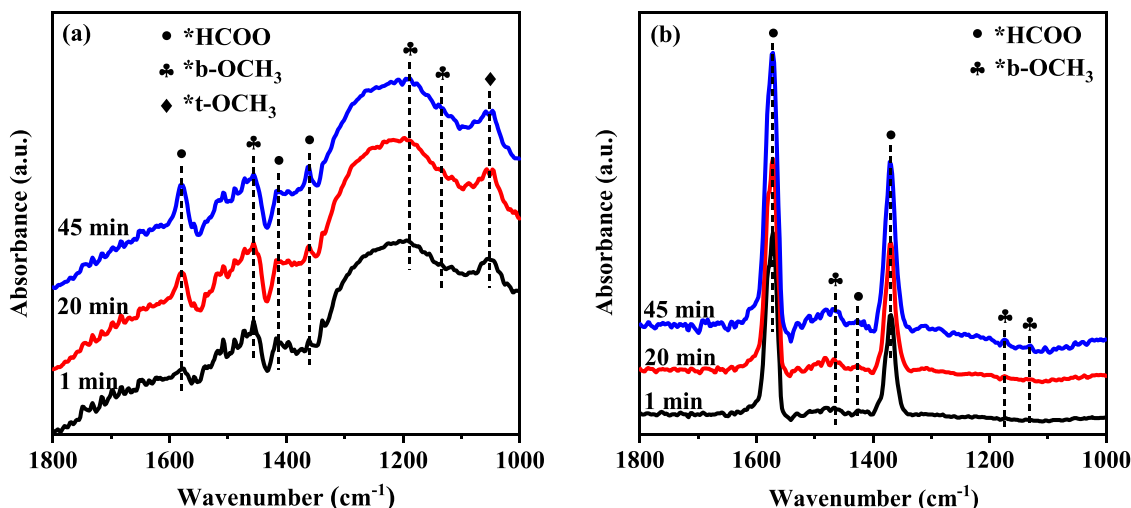


Fig. 6. In situ DRIFTS spectra of the Cu/ZnO (a) and  $\text{Au}_{0.005}\text{Cu}/\text{ZnO}$  (b) catalysts as a function of reaction time at 250 °C.

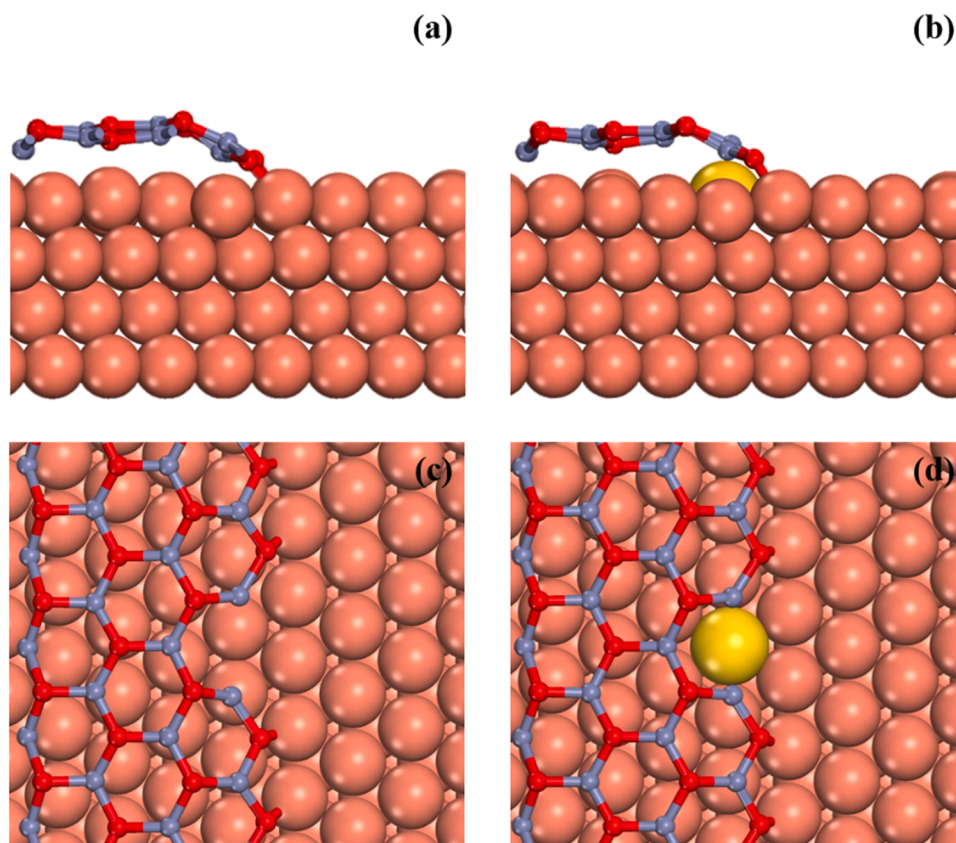


Fig. 7. Side view (upper panels) and top view (lower panels) of the  $\text{ZnO}_{1-x}/\text{Cu}(111)$  (a, c) and  $\text{ZnO}_{1-x}/\text{Au-Cu}(111)$  (b, d) models. The vermilion, red, gray blue and yellow balls represent Cu, O, Zn and Au atoms, respectively.

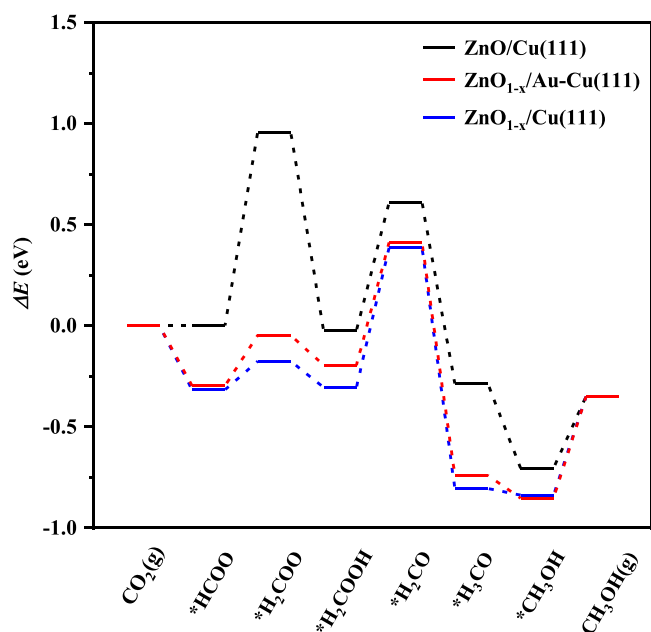


Fig. 8. Reaction energy profiles of  $\text{CO}_2$  hydrogenation to methanol on the  $\text{ZnO}/\text{Cu}(111)$ ,  $\text{ZnO}_{1-x}/\text{Au-Cu}(111)$  and  $\text{ZnO}_{1-x}/\text{Cu}(111)$  surface. The  $\text{ZnO}_{1-x}/\text{Cu}(111)$  surface served as a reference model.

induce more oxygen vacancies and thus facilitate the conversion of reactants/intermediates, leading to boosted methanol synthesis activity.

Third, various adsorption configurations of methoxy species on the  $\text{Cu}/\text{ZnO}$  and  $\text{Au}_x\text{Cu}/\text{ZnO}$  catalysts were comparatively simulated.

Similar to the calculation of reaction energy, the  $\text{ZnO}/\text{Cu}(111)$  and  $\text{ZnO}_{1-x}/\text{Au-Cu}(111)$  models were used as the start surface for adsorption simulations. DFT calculations revealed that both *b*- $\text{CH}_3\text{O}$  and *t*- $\text{CH}_3\text{O}$  species could be stably adsorbed on the  $\text{ZnO}/\text{Cu}(111)$  surface. In contrast, only adsorption of *b*- $\text{CH}_3\text{O}$  species was found on the  $\text{ZnO}_{1-x}/\text{Au-Cu}(111)$  surface. The stabilized adsorption configurations of methoxy species were presented in Fig. 9. Specifically, *b*- $\text{CH}_3\text{O}$  and *t*- $\text{CH}_3\text{O}$  species adsorbed on Zn edge and O edge of the  $\text{ZnO}/\text{Cu}(111)$  surface respectively. The *b*- $\text{CH}_3\text{O}$  species adsorbed on O edge of the  $\text{ZnO}_{1-x}/\text{Au-Cu}(111)$  surface. Moreover, the adsorption energy ( $E_{\text{ads}}$ ) of various adsorption configurations of methoxy species was compiled in Table S4. It is noted that the  $E_{\text{ads}}$  of *b*- $\text{CH}_3\text{O}$  on the  $\text{ZnO}_{1-x}/\text{Au-Cu}(111)$  surface was noticeably lower than that of *b*- $\text{CH}_3\text{O}$  or *t*- $\text{CH}_3\text{O}$  on the  $\text{ZnO}/\text{Cu}(111)$  surface, suggesting preferred adsorption of *b*- $\text{CH}_3\text{O}$  on the  $\text{Au}_x\text{Cu}/\text{ZnO}$  bimetallic catalysts. DFT calculations document that the adsorption configurations of methoxy species would be effectively modulated after introducing Au into  $\text{Cu}/\text{ZnO}$  catalysts, in consistent with in situ DRIFTS spectra of the  $\text{Cu}/\text{ZnO}$  and  $\text{Au}_{0.005}\text{Cu}/\text{ZnO}$  catalysts.

Last, to gain insight into the charge state of Au, Bader charge of Au before and during reaction was analyzed using the  $\text{ZnO}_{1-x}/\text{Au-Cu}(111)$  model. As compiled in Table S5, the doped Au presented a negative charge of  $-0.67 |e|$ , in consistence with the high electronegativity of Au. Moreover, limited change in charge state of Au was observed during the hydrogenation process. This observation may be rationalized by the fact that Au dopant didn't directly contact with reactants and intermediates. The optimized structure of reactants and intermediates on the  $\text{ZnO}_{1-x}/\text{Au-Cu}(111)$  surface provides explicit evidence for the inertness of Au (Fig. S7).

On the basis of experimental results and theoretical studies, reaction mechanism of  $\text{CO}_2$  hydrogenation to methanol over the  $\text{Cu}/\text{ZnO}$  and  $\text{Au}_x\text{Cu}/\text{ZnO}$  catalysts was proposed in Fig. 10. Over both un-promoted and Au-promoted  $\text{Cu}/\text{ZnO}$  catalysts, methanol synthesis followed a

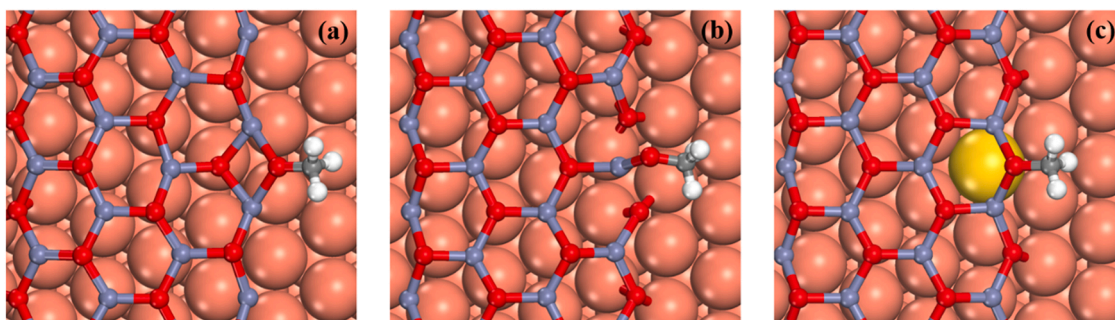


**Fig. 9.** Top view of various adsorption configurations of methoxy species. (a) b-CH<sub>3</sub>O adsorbed on Zn edge of ZnO/Cu(111); (b) t-CH<sub>3</sub>O adsorbed on O edge of ZnO/Cu(111); and (c) b-CH<sub>3</sub>O adsorbed on O edge of ZnO<sub>1-x</sub>/Au-Cu(111). The vermilion, red, gray blue and yellow balls represent Cu, O, Zn and Au atoms, respectively.

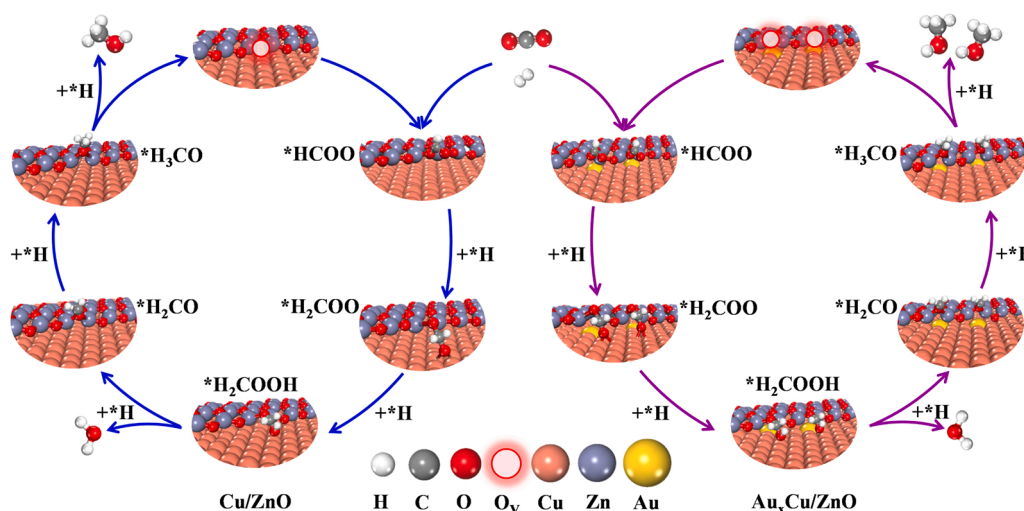


**Fig. 10.** Reaction mechanism of CO<sub>2</sub> hydrogenation to methanol over the Cu/ZnO (left) and Au<sub>x</sub>Cu/ZnO (right) catalysts.

formate pathway, which is consistent with previous studies over Cu-based catalysts [7,24,29]. Furthermore, metal-oxide interfaces with oxygen vacancies were identified as intrinsic active sites. After introducing appropriate amount of Au into Cu/ZnO catalysts, Au-Cu alloy with homogeneous composition was formed. The promotion effect of Au in bimetallic catalysts could mainly be summarized in four aspects. First, the addition of Au would decrease the metal particle size, generating more metal-oxide interfaces. Second, the introduction of Au would induce more oxygen vacancies, yielding more active sites. Third, the incorporation of Au would enrich medium basic sites, promoting the activation of CO<sub>2</sub> molecules. Fourth, the formation of Au-Cu alloy may modulate the adsorption configuration of methoxy intermediates, leading to more effective reaction route. The above promotion effects over the bimetallic Au<sub>x</sub>Cu/ZnO catalysts would work synergistically and result in boosted methanol synthesis activity.

### 3.4. Stability of the Au<sub>0.005</sub>Cu/ZnO catalyst

The long-term stability of the Au<sub>0.005</sub>Cu/ZnO catalyst, the optimal one, was tested at 250 °C for 30 h. As documented in Fig. S8, the Au<sub>0.005</sub>Cu/ZnO catalyst exhibited excellent long-term stability. Specifically, CO<sub>2</sub> conversion maintained around 6.4 % with a fluctuation range of  $\pm 0.2$  %. Methanol selectivity and  $STY_{MeOH}$  increased slightly from 57.7 % and 314.4 g<sub>MeOH</sub> kg<sub>cat</sub><sup>-1</sup> h<sup>-1</sup> to 58.9 % and 320.7 g<sub>MeOH</sub> kg<sub>cat</sub><sup>-1</sup> h<sup>-1</sup>, respectively. The exceptional initial activity and excellent long-term stability endow the Au<sub>0.005</sub>Cu/ZnO catalyst as one of competitive candidates for the industrial catalysts. In addition, TEM measurement was carried out to characterize the spent Au<sub>0.005</sub>Cu/ZnO catalyst. As shown in Fig. S9, the metal nanoparticles on the spent catalyst exhibited the

same lattice distance as those on the fresh sample (Fig. 3c), suggesting the preservation of Au-Cu alloy structure during the stability test. Moreover, the average size of Au-Cu alloy nanoparticles on the spent catalyst was estimated to be 17.9 nm, which was close to that on the fresh sample (17.7 nm). The above results indicate that Au-Cu alloy was stable without evident metal sintering after 30 h of reaction.

## 4. Conclusions

A series of Au<sub>x</sub>Cu/ZnO bimetallic catalysts with various Au/Cu molar ratio ( $x = 0.001, 0.005, 0.02$  and  $0.05$ ) were prepared by the facile co-precipitation method for methanol synthesis via CO<sub>2</sub> hydrogenation. Compared with the Cu/ZnO monometallic catalyst, the Au<sub>x</sub>Cu/ZnO bimetallic catalysts exhibited close CO<sub>2</sub> conversion but boosted methanol selectivity and  $STY_{MeOH}$ . The  $STY_{MeOH}$  on the Au<sub>0.005</sub>Cu/ZnO catalyst reached 314.4 g<sub>MeOH</sub> kg<sub>cat</sub><sup>-1</sup> h<sup>-1</sup> at 250 °C under 3.0 MPa, which was 1.75 times as high as that on the Cu/ZnO catalyst (179.7 g<sub>MeOH</sub> kg<sub>cat</sub><sup>-1</sup> h<sup>-1</sup>). Structural characterizations identify the formation of Au-Cu alloy after introducing appropriate amount of Au into Cu/ZnO catalysts. The Au<sub>x</sub>Cu/ZnO bimetallic catalysts exhibited higher  $S_{BET}$ , smaller metal particle size, more oxygen vacancies, stronger metal-support interactions and more abundant medium basic sites than the Cu/ZnO monometallic catalyst. In situ DRIFTS spectra and DFT calculations suggest a formate pathway for methanol synthesis on both un-promoted and Au-promoted Cu/ZnO catalysts. Metal-oxide interfaces decorated with oxygen vacancies were inferred as intrinsic active sites. The addition of Au would generate more active sites, promote CO<sub>2</sub> activation and modify intermediate conversion, synergistically leading to boosted methanol synthesis activity. Besides, the Au<sub>0.005</sub>Cu/ZnO catalyst was

stable for 30 h of reaction at 250 °C. The present work for the first time demonstrates the promotion effect of Au on Cu/ZnO catalysts for methanol synthesis via CO<sub>2</sub> hydrogenation. It is worth emphasizing that the trace amount of Au addition (only 0.4 wt% in the Au<sub>0.005</sub>Cu/ZnO catalyst) would favor the industrialization of the AuCu bimetallic catalysts in the future.

### CRedit authorship contribution statement

**Guiming Xie:** Methodology, Investigation, Writing - Original Draft. **Rongrong Jin:** Validation, Formal analysis, Writing-Review & Editing. **Pengju Ren:** Supervision, Methodology, Data Curation. **Yunming Fang:** Supervision, Data Curation, Funding acquisition. **Runduo Zhang:** Methodology, Data Curation, Resources. **Zhou-jun Wang:** Conceptualization, Supervision, Funding acquisition.

### Declaration of Competing Interest

The authors declare that they have no known competing financial interests or personal relationships that could have appeared to influence the work reported in this paper.

### Data availability

Data will be made available on request.

### Acknowledgments

The financial support from National Natural Science Foundation of China (21776007, 21811530293) and National Key Research and Development Project (2018YFB1501405) are acknowledged.

### Appendix A. Supporting information

Supplementary data associated with this article can be found in the online version at doi:10.1016/j.apcatb.2022.122233.

### References

- [1] A. Guterres, Carbon neutrality by 2050: The world's most urgent mission. (<https://www.un.org/sg/en/content/sg/articles/2020-12-11/carbonneutrality-2050-the-world%E2%80%99s-most-urgent-mission>) (accessed 28 July, 2022).
- [2] U.S. Environmental Protection Agency, Overview of greenhouse gases, (<https://www.epa.gov/ghgemissions/overview-greenhouse-gases>) (accessed 28 July, 2022).
- [3] Z.-j. Wang, H. Song, H. Liu, J. Ye, Coupling of solar energy and thermal energy for carbon dioxide reduction: status and prospects, *Angew. Chem. Int. Ed.* 59 (2020) 8016–8035.
- [4] H. Ham, S.W. Baek, C.-H. Shin, J.W. Bae, Roles of structural promoters for direct CO<sub>2</sub> hydrogenation to dimethyl ether over ordered mesoporous bifunctional Cu/M-Al<sub>2</sub>O<sub>3</sub> (M = Ga or Zn), *ACS Catal.* 9 (2019) 679–690.
- [5] J. Guo, Z. Wang, J. Li, Z. Wang, In-Ni intermetallic compounds derived from layered double hydroxides as efficient catalysts toward the reverse water gas shift reaction, *ACS Catal.* 12 (2022) 4026–4036.
- [6] N. Rui, F. Zhang, K. Sun, Z. Liu, W. Xu, E. Stavitski, S.D. Senanayake, J. A. Rodriguez, C.-J. Liu, Hydrogenation of CO<sub>2</sub> to methanol on a Au<sup>δ+</sup>-In<sub>2</sub>O<sub>3-x</sub> catalyst, *ACS Catal.* 10 (2020) 11307–11317.
- [7] Z.-j. Wang, H. Song, H. Pang, Y. Ning, T.D. Dao, Z. Wang, H. Chen, Y. Weng, Q. Fu, T. Nagao, Y. Fang, J. Ye, Photo-assisted methanol synthesis via CO<sub>2</sub> reduction under ambient pressure over plasmonic Cu/ZnO catalysts, *Appl. Catal. B Environ.* 250 (2019) 10–16.
- [8] A.R. Richard, M.H. Fan, Low-pressure hydrogenation of CO<sub>2</sub> to CH<sub>3</sub>OH using Ni-In-Al/SiO<sub>2</sub> catalyst synthesized via a phyllosilicate precursor, *ACS Catal.* 7 (2017) 5679–5692.
- [9] X. Wang, H. Zhang, Kinetically relevant variation triggered by hydrogen pressure: a mechanistic case study of CO<sub>2</sub> hydrogenation to methanol over Cu/ZnO, *J. Catal.* 406 (2022) 145–156.
- [10] X. Jiang, X. Nie, X. Guo, C. Song, J.G. Chen, Recent advances in carbon dioxide hydrogenation to methanol via heterogeneous catalysis, *Chem. Rev.* 120 (2020) 7984–8034.
- [11] J. Zhong, X. Yang, Z. Wu, B. Liang, Y. Huang, T. Zhang, State of the art and perspectives in heterogeneous catalysis of CO<sub>2</sub> hydrogenation to methanol, *Chem. Soc. Rev.* 49 (2020) 1385–1413.
- [12] E. Lam, G. Noh, K. Larmier, O.V. Safonova, C. Copéret, CO<sub>2</sub> hydrogenation on Cu-catalysts generated from ZnII single-sites: Enhanced CH<sub>3</sub>OH selectivity compared to Cu/ZnO/Al<sub>2</sub>O<sub>3</sub>, *J. Catal.* 394 (2021) 266–272.
- [13] N. Li, W. Wang, L. Song, H. Wang, Q. Fu, Z. Qu, CO<sub>2</sub> hydrogenation to methanol promoted by Cu and metastable tetragonal Ce<sub>x</sub>Zr<sub>y</sub>O<sub>2</sub> interface, *J. Energy Chem.* 68 (2022) 771–779.
- [14] M.M.-J. Li, S.C.E. Tsang, Bimetallic catalysts for green methanol production via CO<sub>2</sub> and renewable hydrogen: a mini-review and prospects, *Catal. Sci. Technol.* 8 (2018) 3450–3464.
- [15] X. Jiang, N. Koizumi, X. Guo, C. Song, Bimetallic Pd-Cu catalysts for selective CO<sub>2</sub> hydrogenation to methanol, *Appl. Catal. B Environ.* 170–171 (2015) 173–185.
- [16] X. Jiang, X. Nie, X. Wang, H. Wang, N. Koizumi, Y. Chen, X. Guo, C. Song, Origin of Pd-Cu bimetallic effect for synergistic promotion of methanol formation from CO<sub>2</sub> hydrogenation, *J. Catal.* 369 (2019) 21–32.
- [17] S. Tada, F. Watanabe, K. Kiyota, N. Shimoda, R. Hayashi, M. Takahashi, A. Nariyuki, A. Igarashi, S. Satokawa, Ag addition to CuO-ZrO<sub>2</sub> catalysts promotes methanol synthesis via CO<sub>2</sub> hydrogenation, *J. Catal.* 351 (2017) 107–118.
- [18] Q. Tan, Z. Shi, D. Wu, CO<sub>2</sub> hydrogenation to methanol over a highly active Cu-Ni/CeO<sub>2</sub>-nanotube catalyst, *Ind. Eng. Chem. Res.* 57 (2018) 10148–10158.
- [19] Y. Hartadi, D. Widmann, R.J. Behm, Methanol formation by CO<sub>2</sub> hydrogenation on Au/ZnO catalysts-effect of total pressure and influence of CO on the reaction characteristics, *J. Catal.* 333 (2016) 238–250.
- [20] A. Vourros, I. Garagounis, V. Kyriakou, S.A.C. Carabineiro, F.J. Maldonado-Hódar, G.E. Marnellos, M. Konsolakis, Carbon dioxide hydrogenation over supported Au nanoparticles: effect of the support, *J. CO<sub>2</sub> Util.* 19 (2017) 247–256.
- [21] K.S.W. Sing, D.H. Everett, R.A.W. Haul, L. Moscou, R.A. Pierotti, J. Rouquerol, T. Siemieniowska, Physisorption data for gas/solid systems with special reference to the determination of surface area and porosity, *Pure Appl. Chem.* 57 (1985) 603–619.
- [22] A.M. Abdel-Mageed, M. Büselmann, K. Wiese, C. Fauth, R.J. Behm, Influence of water vapor on the performance of Au/ZnO catalysts in methanol synthesis from CO<sub>2</sub> and H<sub>2</sub>: a high-pressure kinetic and TAP reactor study, *Appl. Catal. B Environ.* 297 (2021), 120416.
- [23] W. Wang, Z. Qu, L. Song, Q. Fu, CO<sub>2</sub> hydrogenation to methanol over Cu/CeO<sub>2</sub> and Cu/ZrO<sub>2</sub> catalysts: tuning methanol selectivity via metal-support interaction, *J. Energy Chem.* 40 (2020) 22–30.
- [24] M. Behrens, R. Schlögl, How to prepare a good Cu/ZnO catalyst or the role of solid state chemistry for the synthesis of nanostructured catalysts, *Z. Anorg. Allg. Chem.* 639 (2013) 2683–2695.
- [25] X. Yang, H. Chen, Q. Meng, H. Zheng, Y. Zhu, Y. Li, Insights into influence of nanoparticle size and metal-support interactions of Cu/ZnO catalysts on activity for furfural hydrogenation, *Catal. Sci. Technol.* 7 (2017) 5625–5634.
- [26] X.-W. Lv, L. Wang, G. Wang, R. Hao, J.-T. Ren, X. Liu, P.N. Duchesne, Y. Liu, W. Li, Z.-Y. Yuan, G.A. Ozin, ZIF-supported AuCu nanoalloy for ammonia electrosynthesis from nitrogen and thin air, *J. Mater. Chem. A* 8 (2020) 8868–8874.
- [27] D. Jiang, Y. Zhou, Q. Zhang, Q. Song, C. Zhou, X. Shi, D. Li, Synergistic integration of AuCu co-catalyst with oxygen vacancies on TiO<sub>2</sub> for efficient photocatalytic conversion of CO<sub>2</sub> to CH<sub>4</sub>, *ACS Appl. Mater. Interfaces* 13 (2021) 46772–46782.
- [28] S. Kattel, P. Liu, J.G. Chen, Tuning selectivity of CO<sub>2</sub> hydrogenation reactions at the metal/oxide interface, *J. Am. Chem. Soc.* 139 (2017) 9739–9754.
- [29] K. Larmier, W.-C. Liao, S. Tada, E. Lam, R. Verel, A. Bansode, A. Urakawa, A. Comas-Vives, C. Copéret, CO<sub>2</sub>-to-methanol hydrogenation on zirconia-supported copper nanoparticles: reaction intermediates and the role of the metal-support interface, *Angew. Chem. Int. Ed.* 56 (2017) 2318–2323.
- [30] Y. Yu, X. Dong, P. Chen, Q. Geng, H. Wang, J. Li, Y. Zhou, F. Dong, Synergistic effect of Cu single atoms and Au-Cu alloy nanoparticles on TiO<sub>2</sub> for efficient CO<sub>2</sub> photoreduction, *ACS Nano* 15 (2021) 14453–14464.
- [31] X. Bai, G. Xie, Y. Guo, L. Tian, H.M. El-Hosainy, A.E. Awadallah, S. Ji, Z.-J. Wang, A highly active Ni catalyst supported on Mg-substituted LaAlO<sub>3</sub> for carbon dioxide reforming of methane, *Catal. Today* 368 (2021) 78–85.
- [32] H. Arandiyán, H. Dai, J. Deng, Y. Liu, B. Bai, Y. Wang, X. Li, S. Xie, J. Li, Three-dimensionally ordered macroporous La<sub>0.6</sub>Sr<sub>0.4</sub>MnO<sub>3</sub> with high surface areas: active catalysts for the combustion of methane, *J. Catal.* 307 (2013) 327–339.
- [33] T.S. Rodrigues, A.B.L. de Moura, F.Ae Silva, E.G. Candido, A.G.M. da Silva, D.C. de Oliveira, J. Quiroz, P.H.C. Camargo, V.S. Bergamaschi, J.C. Ferreira, M. Linardi, F. C. Fonseca, Ni supported Ce<sub>0.9</sub>Sm<sub>0.1</sub>O<sub>2-δ</sub> nanowires: an efficient catalyst for ethanol steam reforming for hydrogen production, *Fuel* 237 (2019) 1244–1253.
- [34] J. Zhu, D. Ciolca, L. Liu, A. Parastaev, N. Kosinov, E.J.M. Hensen, Flame synthesis of Cu/ZnO-CeO<sub>2</sub> catalysts: synergistic metal-support interactions promote CH<sub>3</sub>OH selectivity in CO<sub>2</sub> hydrogenation, *ACS Catal.* 11 (2021) 4880–4892.
- [35] X. Liao, W. Chu, X. Dai, V. Pitchon, Bimetallic Au-Cu supported on ceria for PROX reaction: effects of Cu-Au atomic ratios and thermal pretreatments, *Appl. Catal. B Environ.* 142–143 (2013) 25–37.
- [36] K.-J. Kim, H.-G. Ahn, Complete oxidation of toluene over bimetallic Pt-Au catalysts supported on ZnO/Al<sub>2</sub>O<sub>3</sub>, *Appl. Catal. B Environ.* 91 (2009) 308–318.
- [37] M.-H. Liu, Y.-W. Chen, T.-S. Lin, C.-Y. Mou, Defective mesocrystal ZnO-supported gold catalysts: facilitating CO oxidation via vacancy defects in ZnO, *ACS Catal.* 8 (2018) 6862–6869.
- [38] J. Sun, Y. Wang, H. Zou, X. Guo, Z.-J. Wang, Ni catalysts supported on nanosheet and nanoplate γ-Al<sub>2</sub>O<sub>3</sub> for carbon dioxide methanation, *J. Energy Chem.* 29 (2019) 3–7.
- [39] Y. Sun, C. Huang, L. Chen, Y. Zhang, M. Fu, J. Wu, D. Ye, Active site structure study of Cu/plate ZnO model catalysts for CO<sub>2</sub> hydrogenation to methanol under the real reaction conditions, *J. CO<sub>2</sub> Util.* 37 (2020) 55–64.

- [40] W.-G. Cui, Y.-T. Li, L. Yu, H. Zhang, T.-L. Hu, Zeolite-encapsulated ultrasmall Cu/ZnO<sub>x</sub> nanoparticles for the hydrogenation of CO<sub>2</sub> to methanol, *ACS Appl. Mater. Interfaces* 13 (2021) 18693–18703.
- [41] K. Chang, T. Wang, J.G. Chen, Hydrogenation of CO<sub>2</sub> to methanol over CuCeTiO<sub>x</sub> catalysts, *Appl. Catal. B Environ.* 206 (2017) 704–711.
- [42] Y.-L. Fang, J. Zhao, K.N. Heck, L.A. Pretzer, N. Guo, T. Wu, W. Zhang, J.T. Miller, M.S. Wong, Thermal annealing effects on palladium-decorated gold nanoparticle catalysts, *J. Catal.* 410 (2022) 246–255.
- [43] C. Wu, L. Lin, J. Liu, J. Zhang, F. Zhang, T. Zhou, N. Rui, S. Yao, Y. Deng, F. Yang, W. Xu, J. Luo, Y. Zhao, B. Yan, X.-D. Wen, J.A. Rodriguez, D. Ma, Inverse ZrO<sub>2</sub>/Cu as a highly efficient methanol synthesis catalyst from CO<sub>2</sub> hydrogenation, *Nat. Commun.* 11 (2020) 5767.
- [44] K. Chen, H. Fang, S. Wu, X. Liu, J. Zheng, S. Zhou, X. Duan, Y. Zhuang, S.C. E. Tsang, Y. Yuan, CO<sub>2</sub> hydrogenation to methanol over Cu catalysts supported on La-modified SBA-15: the crucial role of Cu-LaO<sub>x</sub> interfaces, *Appl. Catal. B Environ.* 251 (2019) 119–129.
- [45] S. Kattel, B. Yan, Y. Yang, J.G. Chen, P. Liu, Optimizing binding energies of key intermediates for CO<sub>2</sub> hydrogenation to methanol over oxide-supported copper, *J. Am. Chem. Soc.* 138 (2016) 12440–12450.
- [46] W. Wang, Z. Qu, L. Song, Q. Fu, Probing into the multifunctional role of copper species and reaction pathway on copper-cerium-zirconium catalysts for CO<sub>2</sub> hydrogenation to methanol using high pressure in situ DRIFTS, *J. Catal.* 382 (2020) 129–140.
- [47] J. Song, S. Liu, C. Yang, G. Wang, H. Tian, Z.-J. Zhao, R. Mu, J. Gong, The role of Al doping in Pd/ZnO catalyst for CO<sub>2</sub> hydrogenation to methanol, *Appl. Catal. B Environ.* 263 (2020), 118367.
- [48] A. Cao, Z. Wang, H. Li, A.O. Elnabawy, J.S. Nørskov, New insights on CO and CO<sub>2</sub> hydrogenation for methanol synthesis: the key role of adsorbate-adsorbate interactions on Cu and the highly active MgO-Cu interface, *J. Catal.* 400 (2021) 325–331.
- [49] S.-S. Wang, H.-Y. Su, X.-K. Gu, W.-X. Li, Differentiating intrinsic reactivity of copper, copper-zinc alloy and copper/zinc oxide interface for methanol steam reforming by first principles theory, *J. Phys. Chem. C* 121 (2017) 21553–21559.
- [50] X. Liu, J. Luo, H. Wang, L. Huang, S. Wang, S. Li, Z. Sun, F. Sun, Z. Jiang, S. Wei, W.-X. Li, J. Lu, In situ spectroscopic characterization and theoretical calculations identify partially reduced ZnO<sub>1-x</sub>/Cu interfaces for methanol synthesis from CO<sub>2</sub>, *Angew. Chem. Int. Ed.* 61 (2022), e202202330.